Kinetically Controlled Assembly of a Spirocyclic Aromatic Hydrocarbon into Polyhedral Micro/Nanocrystals

Zong-Qiong Lin,[†,‡,⊥] Peng-Ju Sun,[†] Yee-Yan Tay,[‡,§] Jing Liang,[†] Yi Liu,[‡] Nai-En Shi,[†] Ling-Hai Xie,[†,⊥,*] Ming-Dong Yi,[†] Yan Qian,[†] Qu-Li Fan,[†] Hua Zhang,[‡] Huey Hoon Hng,[‡,§] Jan Ma,[‡] Qichun Zhang,[‡,*] and Wei Huang[†,⊥,*]

[†]Key Laboratory for Organic Electronics & Information Displays (KLOEID) and Institute of Advanced Materials (IAM), Nanjing University of Posts and Telecommunications, 9 Wenyuan Road, Nanjing 210046, People's Republic of China, [‡]School of Materials Science and Engineering and [§]Facility for Analysis Characterization, Testing, Simulation (FACTS), Nanyang Technological University, 50 Nanyang Avenue, Singapore 639798, and [⊥]Jiangsu-Singapore Joint Research Center for Organic/Bio Electronics & Information Displays, 9 Wenyuan Road, Nanjing 210046, People's Republic of China

ABSTRACT

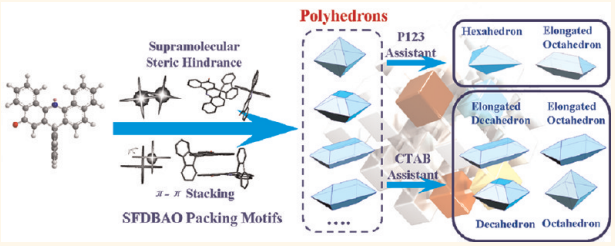

Nonplane molecules with multiple large aromatic planes could be promising candidates to form various polyhedral micro/nanocrystals by manipulating the different $\pi\cdots\pi$ stacking, tuning the cohesive energies of crystal facets, and controlling the kinetic growth process. Spirocyclic aromatic hydrocarbons (SAHs) not only have two cross-shaped aromatic planes but also offer the feature of supramolecular steric hindrance, making it favorable for the heterogeneous kinetic growth into highly symmetric polyhedra. Herein, we report that a novel SAH compound, spiro[fluorene-9,7′-dibenzo[*c*,*h*]acridine]-5′-one (SFDBAO), can self-assemble into various monodispersed shapes such as hexahedra, octahedra, and decahedra through the variation of either different types of surfactants, such as Pluronic 123 (P123) and cetyltrimethyl ammonium bromide (CTAB), or growth parameters. In addition, the possible mechanism of crystal facet growth has been proposed according to the SEM, XRD, TEM, and SAED characterization of organic polyhedral micro/nanocrystals. The unique cruciform-shaped SAHs have been demonstrated as fascinating supramolecular synthons for various highly symmetric polyhedral assembling.

KEYWORDS: cruciform-shaped molecules · spirocyclic aromatic hydrocarbon · supramolecular assembly · polyhedron · kinetic crystal growth · surfactant

Organic polyhedra with diverse shapes, sizes, and compositions are of interest because these factors not only attract fundamental interests but also affect physical properties and their applications in organic nanoelectronics and nanophotonics.[1−23] However, rather weak supramolecular interactions, complicated mechanism of kinetic growth, and the unclear correlation between crystal morphology and molecular configuration make it a great challenge to controllably synthesize a highly symmetric polyhedron from organic synthons.

Unlike the inorganic counterparts, which are formed through covalent bonds, ionic bonds, or metal−metal bonds,[24−28] organic micro/nanostructures usually aggregate together through weak supramolecular interactions. Such assemblies are readily disturbed by environmental factors (*e.g.*, surfactants, solvents, concentration, and temperature). In another word, the morphologies of organic micro/nanocrystals could be controlled by the complicated kinetic growth and/or dynamic molecular assembly, in which organic polyhedral micro/nanostructures are dominated by the competition of crystal facet growth owing to the different cohesive energies induced by surfactants.[29−31] Several reports have already described these effects in detail.[28,30,32,33] For example, Lee *et al.* reported[34] the Pluronic 123 (P123)-assisted assembly of polyhedra from 2,5,8,11-tetra-*tert*-butylperylene into micro/nanocubes, truncated cubes, and rhombic dodecahedra. Kang *et al.*[35] examined the influence of cetyltrimethylammonium bromide (CTAB) and poly(vinyl pyrrolidone) (PVP) on sizes and shapes of organic micro/nanocrystals through the manipulation of the nucleation and the subsequent growth kinetics, respectively.

Furthermore, researchers recently found that the cohesive energy of organic polyhedral crystal surfaces sensitively depends on molecular architectures,[29−31,36] which can be tuned through appropriately engineering the configurations of molecular and supramolecular linkages, such as coordination bonding,[37−39] hydrogen bonding,[40]

* Address correspondence to qczhang@ntu.edu.sg, iamlhxie@njupt.edu.cn, iamwhuang@njupt.edu.cn.

Received for review March 14, 2012 and accepted May 10, 2012.

Published online May 10, 2012
10.1021/nn3011398

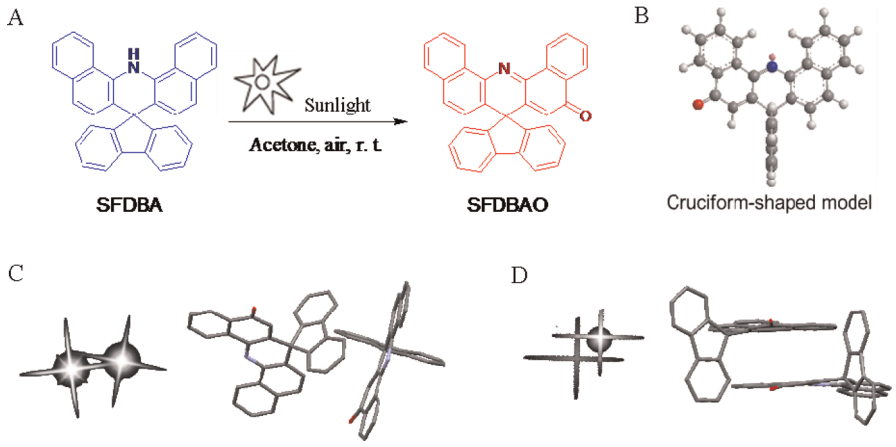

Scheme 1. (A) Synthetic route of SFDBAO. (B) Cruciform-shaped molecular structure of SFDBAO containing two perpendicular aromatic planes: dibenzoacridinone and fluorene. (C) Schematic models with the SSH. (D) Molecular packing arrangements of SFDBAO.

amphiphiles,[41] and $\pi\cdots\pi$ interactions.[42,43] For example, Stupp *et al.*[44] combined the intermolecular $\pi\cdots\pi$ stacking and hydrogen bonding together to kinetically control the long-range orientation of an oligothiophene to form the bundled fibers, rhombohedra, and hexagonal prisms. Kwon and co-workers[45,46] demonstrated that a 3D β-peptide foldamer could act as an excellent scaffold to achieve a tooth shape with the concept of "folding into shape". Hasell *et al.*[47] controllably synthesized the porous cage-like organic nanocrystals from a rigid organic cage module, with nonplanar interactions, by varying the temperatures. However, using nonplanar molecules with multiple large aromatic planes to preferentially self-assemble into the highly symmetric polyhedra is unprecedented. We do believe that nonplane molecules with multiple large aromatic planes could offer us additional factors to control the formation of various polyhedral micro/nanocrystals by manipulating the different $\pi\cdots\pi$ stacking, tuning the cohesive energies of crystal facets, and controlling the kinetic growth process.

To the best of our knowledge, most reported molecules used for making organic micro/nanocrystals only have one main aromatic plane for the $\pi\cdots\pi$ stacking.[14,48−50] In the case of a nonplanar molecule with multiple aromatic planes, the anisotropic cohesive energy will be realized as the directional $\pi\cdots\pi$ stacking from each aromatic plane. Recently, we assembled 9,10-diphenylanthracene (DPA) into octahedral microcrystals[51] because two phenyl groups in the DPA molecule crossly attached to the backbone of anthracene and exhibited three stacking modes with different binding energy in directional $\pi\cdots\pi$ stacking.[52] This result encourages us to employ nonplane molecules with multiple large aromatic planes to control the anisotropic cohesive energy and the growth directions of crystal facets. In this report, we are interested in the cruciform-shaped spirocyclic aromatic hydrocarbons (SAHs), which have two perpendicular conjugated aromatics connected together *via* a common sp^3-hybridized atom. Previously, their supramolecular steric hindrance (SSH) effects, namely, repulsive force from steric bulky planes competing with the intermolecular $\pi\cdots\pi$ stacking attraction in molecule packing, have been well investigated.[53−55] The diverse morphologies of polyhedral structure could be anticipated if the balance of the competition of both driving forces is utilized to equilibrate the growth ratio of crystal facets in self-assembly.

Herein, a novel SAH, spiro[fluorene-9,7′-dibenzo[*c*,*h*]acridine]-5′-one, termed as SFDBAO (structure shown in Scheme 1), has been employed to demonstrate the intrinsic feature of organic polyhedral micro/nanocrystals. We believe that two typical cruciform-shaped planes probably have different driving forces in crystal growth and kinetic speeds in crystal packing. Our results clearly show that a series of polyhedra, ranging from octahedron, elongated octahedron, hexahedron, decahedron, to elongated decahedron, have been obtained by manipulating the kinetic self-assembly, selecting the different $\pi\cdots\pi$ stacking, and tuning the cohesive energies of crystal facets under the assistance of surfactants. This work may provide a facile strategy to design and prepare various polyhedral organic micro/nanocrystals for semiconducting device applications.

RESULTS AND DISCUSSION

Synthesis and Supramolecular Assembly of SFDBAO. The key molecule SFDBAO was synthesized through an eco-friendly visible-light-mediated photooxygenation of spiro[fluorene-9,7′-dibenzo[*c*,*h*]acridine] (SFDBA, Scheme 1, Figure S1 in Supporting Information), which was prepared *via* a concise modified one-pot domino reaction under the condition of phosphoric acid (PPA) according to the reported precedure.[56]

The optimized structure of SFDBAO exhibits a cruciform shape (Scheme 1B), where the two aromatic π-systems (as the conjugated dibenzoacridinone plane and the fluorene plane) are connected *via* a common sp^3-hybridized atom. The two kinds of molecular packing arrangements of SFDBAO are shown in Scheme 1C,D. The perpendicular fluorene moiety provides a unique SSH (Scheme 1C), which is crucial to adjust the packing motifs of SFDBAO out of the simple planar interaction.[14] By tuning the cohesive energy, SFDBAO offers absolutely different anisotropic growth directions from that of classical semiconductors. The dibenzoacridinone plane consists of naphthalene and acridinone moieties, which form a typical intramolecular charge-transfer structure. Such arrangement causes a strong supramolecular dipole−dipole interaction (Scheme 1D), which dramatically enhances the $\pi\cdots\pi$ attraction between two neighbor molecules (naphthalene and acridinone moiety). The cruciform-shape configuration provides an intrinsic anisotropic cohesive energy of SFDBAO in self-assembly. The competition of SSH repulse and $\pi\cdots\pi$ stacking attraction will adjust the packing motifs in molecule arrangement, leading to the anisotropic growth ratio of different crystal facets and the polyhedral structure eventually. As a result, the well-defined polyhedral crystals with high symmetry in micro/nanoscale will be obtained by controlling the kinetic growth process.

In order to examine the intrinsic polyhedral features, we first checked the formation of micro/nanocrystals of SFDBAO through a classical reprecipitation method without any assistance of surfactants. Various polyhedra with non-uniform sizes and shapes were observed by simply injecting 1 mL of tetrahydrofuran (THF) solution (1 mM) of SFDBAO into 5 mL of pure water under vigorous stirring, following aging at 298 K for 24 h. The SEM images in Figure 1 confirmed the formation of several different shapes such as octahedron, elongated octahedron, decahedron, and elongated decahedron. Figure 1D illustrates the schematic diagrams of various morphologies.[57−59] These results indicated that (1) SFDBAO inclines to self-assemble into different polyhedra and (2) these shapes might be selectively controlled through the right choice of experimental conditions such as surfactants, aging times, and concentrations.

Surfactant-Assisted Shape Control of SFDBAO Polyhedra. In order to control the morphologies of micro/nanoparticles, several surfactants such as poly(ethylene glycol)-*block*-poly(propylene glycol)-*block*-poly(ethylene glycol) (P123) non-ionic surfactant or CTAB (cationic surfactant) have been employed. Consequently, the shapes and sizes of polyhedra can be easily adjusted as a function of preparation parameter (*e.g.*, the concentrations of surfactant (C_{P123}/C_{CTAB}), SFDBAO (C_{SFDBAO}), the volume of THF (V_{THF}), and aging time) as summarized in Table S1, which will be further discussed below. All samples were separated *via* centrifugation, followed by the decantation

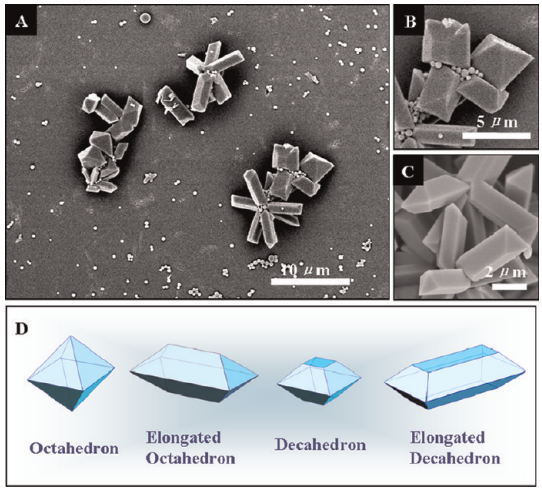

Figure 1. (A) Scanning electron microscopy (SEM) images of SFDBAO micro/nanocrystals reprecipitated from pure water (without any surfactant). (B,C) Highly magnified images of A for the polyhedra observed. (D) Schematic models for the polyhedra: octahedron, elongated octahedron, decahedron, and elongated decahedron.

of the supernatant liquid and washing with distilled water. To confirm their composition and purity, the polyhedra were redissolved in $CDCl_3$ and their ^1H NMR spectra remeasured (Figure S2). All results prove that the as-prepared materials have no change before and after self-assembly. Actually, by washing with water for three times, there was no existence of the residue surfactant on the surface, which could be further proved by FTIR (Figure S3, Supporting Information).

The as-prepared particles were characterized through a typical SEM, and the images are shown in Figure 2. For P123, when 1 mL of 0.5 mM of SFDBAO/THF solution (C_{SFDBAO} = 0.5 mM, V_{THF} = 1 mL) was injected into 5 mL of P123/H_2O solution (C_{P123} = 1 mg/mL), the monodispersed hexahedral crystals (Figure 2A,C) were obtained after 4 h aging. We represent in three perspective views the contour of the uniform hexahedra (Figure 2E), whose edge lengths are recorded as a = 1.02 ± 0.01 μm, b = 755 ± 10 nm, c = 376 ± 10 nm, d = 424 ± 10 nm. The elongated octahedra of SFDBAO were observed when extending the aging time from 4 to 24 h (Figure 2D) without changing any other conditions. As described in the schematic model (Figure 2F), the size parameters are measured as a = 392 ± 10 nm, b = 885 ± 10 nm, c = 469 ± 10 nm, d = 488 ± 10 nm, as well as the aspect ratio of 1.8 (b/d).

Subsequently, when the C_{SFDBAO} was increased to 1 mM (C_{P123} = 1 mg/mL and V_{THF} = 1 mL), the monodispersed elongated octahedra (Figure 2B) were obtained with the parameters as a = 0.90 ± 0.05 μm, b = 1.32 ± 0.05 μm, c = 0.49 ± 0.05 μm, d = 0.60 ± 0.05 μm, $b/d \sim$ 2.2. Furthermore, the size could be as large as b = 2.94 ± 0.05 μm ($b/d \sim$ 2.3) without any shape changing if the C_{SFDBAO} was increased to 2 mM and other factors kept the same (Figure S4). Note that

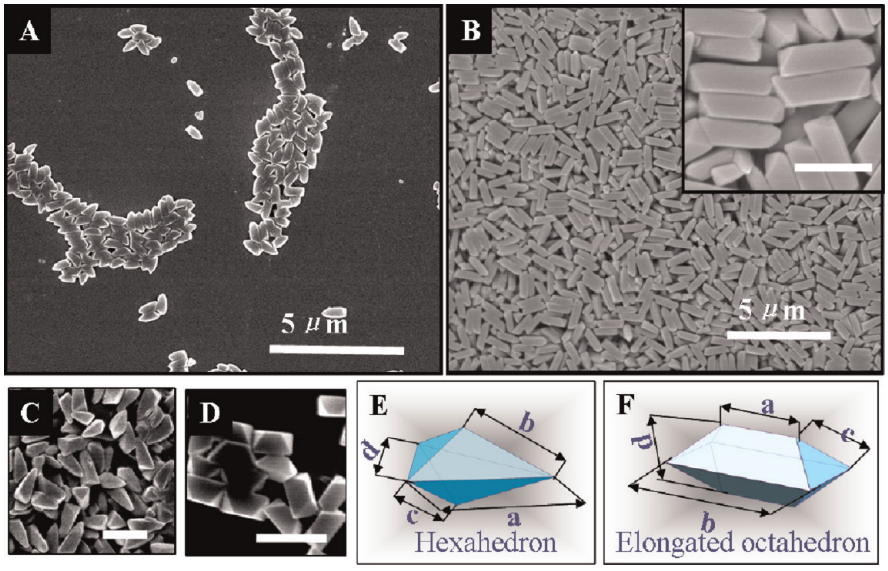

Figure 2. SEM images of (A) hexahedral crystals prepared at C_{SFDBAO} = 0.5 mM, C_{P123} = 1 mg/mL, and V_{THF} = 1 mL, aging time = 4 h. (B) Elongated octahedra prepared at C_{SFDBAO} = 1 mM, C_{P123} = 1 mg/mL, and V_{THF} = 1 mL after 24 h aging. (C) Highly magnified image of A. (D) Elongated octahedra evolve from C after aging for 24 h (scale bars = 1 μm). (E,F) Schematic models of C and D, respectively.

the variation of C_{P123} did affect the sizes and the aspect ratio of elongated octahedra significantly. For example, when the concentration of P123 increases from 1 (shown in Figure 2B) to 2 and to 4 mg/mL without changing other parameters (C_{SFDBAO} = 1 mM and V_{THF} = 1 mL), the sizes of as-obtained particles are b = 1.32, 1.85, and 2.76 ± 0.05 μm, as well as the increase of aspect ratio (b/d = 2.2, 3.2 and 3.5, respectively, Figure S5). A heterogeneous elongated octahedron in size was obtained when C_{P123} = 0.5 mg/mL, with insufficient surfactant (Figure S5A,D). Moreover, when C_{P123} = 4 mg/mL (up to the critical micellization concentration of P123 at 20 °C, CMC[60−63]), the sizes of the obtained elongated octahedra were dramatically increased.[34,46] However, a much longer aging time (about 1 week) was needed. Interestingly, no particles were obtained if C_{P123} was increased to 8 mg/mL. On the other hand, if the V_{THF} decreased to 0.5 mL, nanorods were produced (Figure S6), with the length of ~2.03 μm and the aspect ratio of 7.4. The reason is that, when the concentration of surfactant P123 reaches or passes the CMC, the solubility of SFDBAO will dramatically increase due to the effect of solubilization. At the fixed molar quantity of SFDBAO (C_{SFDBAO} = 1 × 10^{-3} mM, C_{SFDBAO} = 1 mM, V_{THF} = 1 mL) in the system, the supersaturation concentration of SFDBAO in the system becomes much larger, leading to less nucleus being created in the nucleation step. A longer aging time was needed, and much larger polyhedrons were observed. The similar phenomenon was also observed in the reported research for a cube synthesis.[34] In addition, a similar explanation of the critical effect of critical micellization temperature (CMT) was also mentioned in another paper.[46]

The SFDBAO hexahedra and elongated octahedra (from Figure 2) were further characterized by TEM (Figure 3A,D) and selected area electron diffraction (SAED) patterns (Figure 3B,E). Orthorhombic SFDBAO single crystal (obtained from THF/isopropyl alcohol solution) belongs to the space group of $P2(1)2(1)2(1)$(19), with cell parameters of a = 11.260(2) Å, b = 12.060(2) Å, c = 16.530(3) Å, a/b = 0.9337, b/c = 0.7296, c/a = 1.4680, whereas the micro/nanopolyhedra exhibit another phase of monoclinic crystal, with analogical cell parameters of a = 11.295 Å, b = 11.740 Å, c = 17.480 Å, $\alpha = \beta$ = 90.00°, γ = 89.50° (see Supporting Information). The corresponding SAED patterns with remarkable bright regular spots designate the single crystal of the polyhedra from P123. In Figure 3B, the squared and circled sets of spots with d spacing values of 4.87 Å are due to $\{02\bar{2}\}$s (including $\{02\bar{2}\}$ and $\{0\bar{2}2\}$) and $\{30\bar{2}\}$s (including $\{30\bar{2}\}$ and $\{\bar{3}02\}$) Bragg reflections ($d\{02\bar{2}\}$s = 4.87 Å, $d\{30\bar{2}\}$s = 3.46 Å, and $\angle\{02\bar{2}\}/\{30\bar{2}\}$ = 77.65°); thereby, "△" sets of spots with lattice spacing values of 3.16 Å are assigned to reflections from $\{3\bar{2}0\}$s (including $\{3\bar{2}0\}$ and $\{\bar{3}02\}$) crystal planes ($d\{3\bar{2}0\}$s = 3.16 Å and $\angle\{3\bar{2}0\}/\{02\bar{2}\} = \angle\{02\bar{2}\}/\{30\bar{2}\} + \angle\{30\bar{2}\}/\{3\bar{2}0\}$ = 102.35°). In Figure 3E, the "◇", "○", and "▽" sets of spots with d spacing values of 9.49, 7.41, and 5.87 Å are due to $\{10\bar{1}\}$s (including $\{10\bar{1}\}$ and $\{\bar{1}01\}$), $\{11\bar{1}\}$s (including $\{11\bar{1}\}$ and $\{\bar{1}\bar{1}1\}$), and $\{020\}$s (including $\{020\}$ and $\{0\bar{2}0\}$) Bragg reflections ($d\{10\bar{1}\}$s = $d\{101\}$s = 9.49 Å, $d\{11\bar{1}\}$s = $d\{\bar{1}11\}$s = 7.41 Å, $d\{020\}$s = 5.87 Å), and the angles between the reflections are recorded as $\angle\{10\bar{1}\}/\{11\bar{1}\}$ = 51.31°, $\angle\{10\bar{1}\}/\{020\} = \angle\{10\bar{1}\}/\{11\bar{1}\} + \angle\{11\bar{1}\}/\{020\}$ = 89.58°. The schematic models for both of the hexahedra and elongated octahedra with the indexed facets are illustrated in Figure 3C,F.

A different morphology evolution pathway of polyhedral SFDBAO micro/nanocrystals was observed

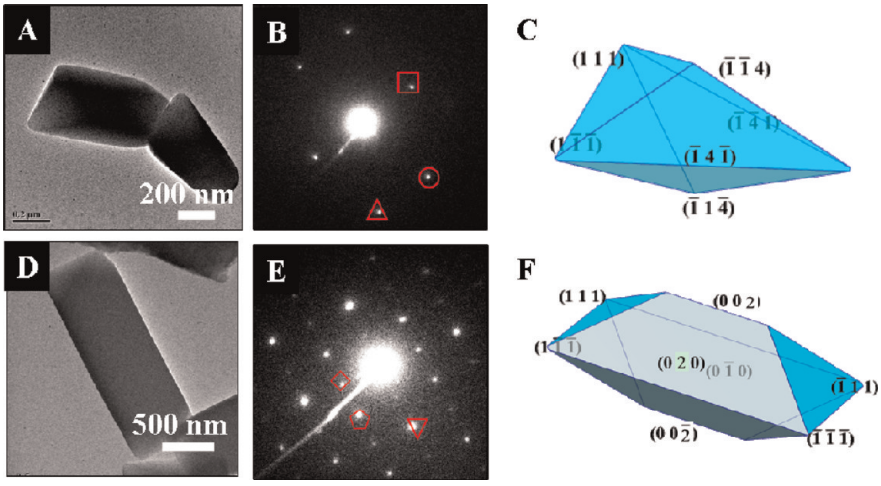

Figure 3. Transmission electron microscopy (TEM) images of hexahedra (A) and elongated octahedra (D). Selected area electron diffraction (SAED) patterns taken from a single elongated octahedron (B) and hexahedra (E). Bragg reflections are denoted by the symbols "□", "○", "△", "◇", "⬠", and "▽", whose Bragg reflections correspond to {02$\bar{2}$}s, {30$\bar{2}$}s, {3$\bar{2}$0}s, {10$\bar{1}$}s, {11$\bar{1}$}s, and {020}s series of facets (with *d* spacing values of 4.87, 3.46, 3.16, 9.49, 7.41, and 5.87 Å), respectively. (C,F) Schematic model for the polyhedra.

when CTAB, a cationic surfactant, was used. As shown in Figure 4, three different shapes were obtained under different conditions. For example, when C_{CTAB} = 0.5 mg/mL (below the CMC at 20 °C,[63,64] C_{SFDBAO} = 0.5 mM, V_{THF} = 1 mL), SFDBAO molecules prefer to self-assemble into a homogeneous elongated decahedral structure after 4 h aging, as shown in Figure 4A, and subsequently convert into elongated octahedral crystals after aging for 48 h (right bottom inset of A). The parameters of elongated decahedra, as described in Figure 4D, are measured as $a = 4.71 \pm 0.05$ μm, $b = 1.45 \pm 0.05$ μm, $c = 575 \pm 50$ nm, and $d = 3.85 \pm 0.05$ μm. Note that if the concentration of CTAB increased into 1 mg/mL, decahedra (truncated octahedra) with inhomogeneous sizes (Figure 4B) were obtained. The dominantly decahedral nano/microcrystals afforded a square on its cross section after initiated 4 h aging and further evolves into the elongated octahedrons with ~48 h aging (right bottom inset of Figure 4B). Interestingly, by simply increasing the concentration of CTAB (C_{CTAB} = 2, 4, 6 mg/mL, C_{SFDBAO} = 1 mM, V_{THF} = 1 mL), the elongated octahedra without uniform size could also be obtained (Figure S7). Only the concentration of CTAB reached 8 mg/mL, and the as-prepared mixtures were aged for 48 h, the uniform SFDBAO octahedra (Figure 4C) were formed. The edge lengths of octahedra (Figure 4C,D) are approximately 600 nm ($a = 673 \pm 10$ nm, $b = 592 \pm 10$ nm). If C_{CTAB} = 0.5 mg/mL (C_{SFDBAO} = 1 mM, V_{THF} = 1 mL), the as-prepared polyhedra remained decahedra (Figure S7A). Interestingly, when C_{CTAB} is fixed at 8 mg/mL, the sizes of the octahedra have no change even if the concentration of SFDBAO was increased up to 2 mM (V_{THF} = 1 mL), but a much sharper edge of octahedron was observed (Figure S8A). Moreover, if the volume of THF (C_{SFDBAO} = 1 mM, C_{CTAB} = 8 mg/mL) decreased, the uniform morphology would become disordered as mentioned before (Figure S8B, Supporting Information). Note that further increasing the concentration of CTAB or the volume of THF caused no precipitation.

The polyhedral structures of SFDBAO from the CTAB system were further characterized by TEM (Figure 5A,D, G). The SAED patterns of elongated decahedron, decahedron, and octahedron are recorded in Figure 5B,E,F. Electronic beam direction is along [1,0,0] in B and E. Note that two new series of spots were observed: one (denoted as the "⬠") with the *d* spacing of 9.75 Å is assigned to {011}s (including {011}and {0$\bar{1}\bar{1}$}) and Bragg reflections (d{011}s = 9.75 Å), and the angle between the reflections is record as $\angle${011}/{020} = 33.89°. The other one, whose *d* spacing value is 8.74 Å (denoted as the "☆"), almost perpendicular with the{020}, was assigned as {002}s (including {002}and{00$\bar{2}$}, d{002}s = 8.74 Å, $\angle${002}/$\angle${020} = $\angle${011}/{002} + $\angle${011}/{020} = 90.00°). As electronic beam direction along [1,0,0] in Figure 5F, a series of {10$\bar{1}$}s, {11$\bar{1}$}s, and {020}s diffraction spots are observed, the same as that of Figure 3B. The details of electron diffraction analysis are shown in Supporting Information.

On the basis of the SAED analyses (Figure 3B,E and Figure 5B,E,H), it could be concluded that these polyhedral nano/microcrystals are single crystals. The results were furthermore confirmed by the results of X-ray diffraction (XRD). It was found that all of the polyhedra suffered identical well-defined XRD profiles, with almost the same peak positions, with distinct different intensities (Figure 6). The *d* spacing values of {101}s, {002}s, {111}s ({11$\bar{1}$}s), {202}s, and {114}s are 9.49, 8.71, 7.41, 4.74, and 3.71 Å, respectively. As evidenced by XRD in the P123 system (Figure 6A), comparison of elongated octahedra (blue line) and

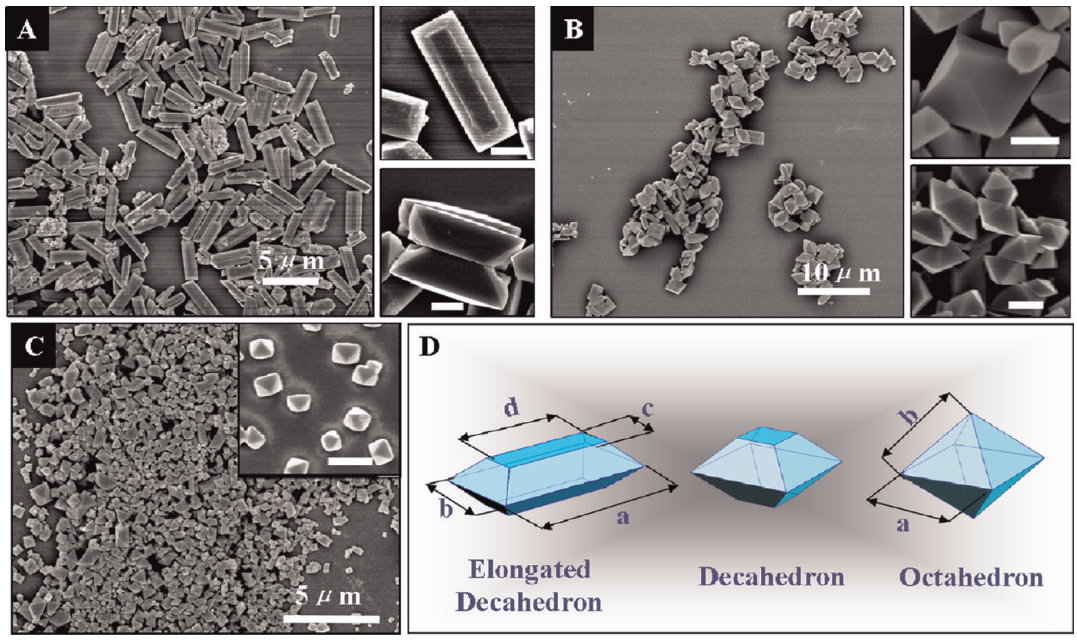

Figure 4. SEM images of (A) elongated decahedra prepared at C_{SFDBAO} = 0.5 mM, C_{CTAB} = 0.5 mg/mL, V_{THF} = 1 mL, aging time = 4 h. (B) Decahedra prepared at C_{SFDBAO} = 1 mM, C_{CTAB} = 1 mg/mL, V_{THF} = 1 mL, aging time = 4 h. (C) Octahedra prepared at C_{SFDBAO} = 1 mM, C_{CTAB} = 8 mg/mL, V_{THF} = 1 mL, aging time = 48 h. The right top inset shows the magnified images of A, B, and C, respectively. The right bottom inset of A and B shows the images of octahedra evolving from the decahedra, after 48 h aging from A and B (scale bars = 1 μm).

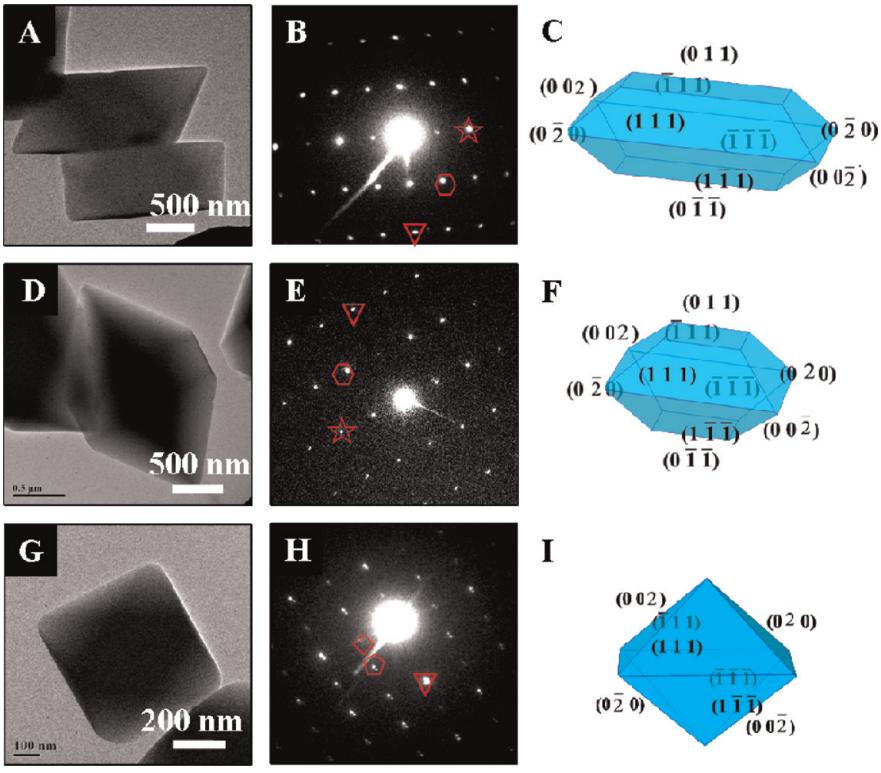

Figure 5. TEM images of (A) elongated decahedron, (D) decahedron, and (G) octahedron. SAED patterns (B,E,H) taken from a single polyhedron. Bragg reflections are denoted by the symbols "⬠", "☆", "▽", "◇", and "⌂", whose Bragg reflections correspond to {011}s, {002}s, {020}s, {10$\bar{1}$}s, and {11$\bar{1}$}s series of facets (with *d* spacing values of 9.75, 8.74, 5.87, 9.49, and 7.41 Å), respectively. (C,F,I) Schematic model for the polyhedra.

hexahedra (red line) showed that the {002}s and {114}s are closely related to the latitude growth. Nevertheless, in the presence of CTAB (Figure 6B), the dramatic increase of the peak intensity of {002}s from the evolution of octahedra (red) to elongated octahedra (blue) supports the longitude growth rather than

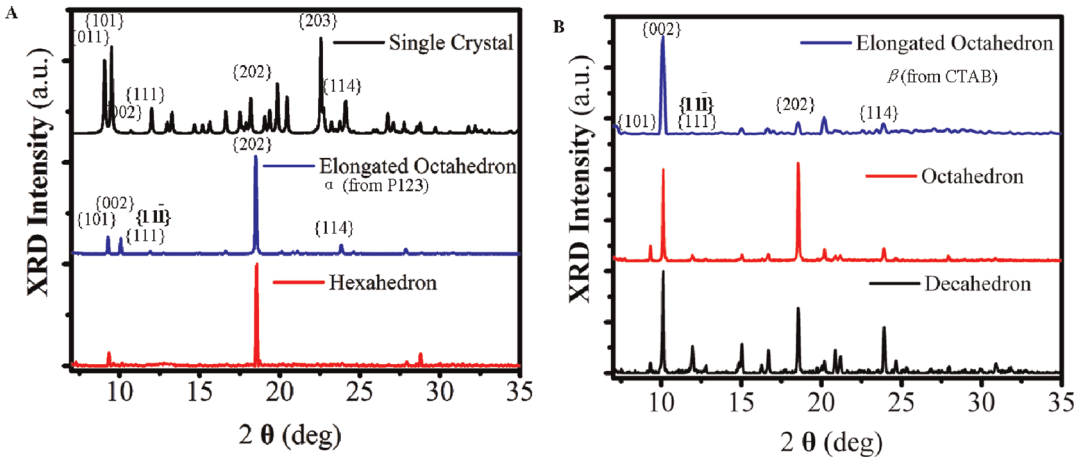

Figure 6. Powder XRD for the polyhedra from P123 (A) and CTAB (B). The corresponding *d* spacing of {101}s, {002}s, {111}s ({11$\bar{1}$}s), {202}s and {114}s facets are 9.49, 8.71, 7.41, 4.74, and 3.71 Å respectively. The top line of A shows the standard powder spectrum simulated on the basis of the single crystal data by using the DIAMOND software.

the latitude growth in P123. Interestingly, compared to the diffraction of both elongated octahedra, {002}s showed much stronger intensity in the CTAB system (Figure 6B, blue), which might suggest a variety of crystal growth directions despite similar morphology after aging (from P123 and CTAB, called elongated octahedron α and β).

Kinetic Growth Mechanisms of SFDBAO Polyhedra. On the basis of our experimental results, a possible transverse mechanism from hexahedra/decahedra to the elongated octahedra/octahedra is proposed (in Scheme 2). As the crystallization is intrinsically a non-equilibrium process, the crystal shapes are mostly dominated by the kinetics of the growth process.[65−68] First of all, we try to index the growing facets of the polyhedra according to the crystallographic data. The XRD data from Figure 6A (the evolution from hexhedra to elongated octahedra) hint that P123 surfactants favor the {111}s growth (blue in color), as well as{114}s, which was further proved by the simulation results of crystal morphology.[57−59] The {002}s are indexed with the purple facets in Scheme 2. Other facets are further indexed by using the software of WinXMorph, and schemed in Figures 3 and 5.

Organic surfactants are one of the most important factors influencing crystal growth in the respect that they would have a strong interaction with the surfaces of growing micro/nanocrystals. The selective adhesion of surfactants at the interface of the surfactant crystal could result in the surface energy difference and lead to the significant differences of growth rate. Although the concrete mechanism dominating the growth trend of the crystal is still unclear yet, so is the unambiguous correlation between intermolecular interactions of SFDBAO and surfactant molecules. We believe that the balance between the $\pi\cdots\pi$ interactions of SFDBAO molecules and hydrophobic interactions between surfactant and SFDBAO molecules plays a significant role. The {114}s are likely to selectively adhere with the P123 micelles, which are surrounded by the PEO hydrophilic shell.[69,70] The selective adhesion to the {114}s can be used to slow down the growth rate of that facet compared to the others (black arrows), leading to the formation of hexahedral crystals, when nucleating seeds formed in the SFDBAO supersaturation. After that, for the high-energy facets of the sharp edge of the hexahedron, the {114}s and {141}s grow more quickly than other facets in such a kinetic regime, eventually forming elongated octahedra α (along the *x* direction). This kinetic growth process is further confirmed by the increase of the aspect ratio as the evolution of the C_{P123} (Figure S5), as the nucleation was surrounded by P123 micelles, and the crystal growth along the latitude was inhibited. We believe that supersaturation degree of SFDBAO will be increased as the volume of THF is decreased and results in a larger amount of nucleus as the seed in small size.[27,32,34,46] The adhesion of P123 at the {114}s facets will inhibit the lattitude growth in the nucleus rather than that of the longitude. As a result, a larger aspect ratio of nanorod morphology was obtained instead of the short elongated octahedron when V_{THF} decreased (Figure S6).

However, if the cationic CTAB is exploited in the investigation, it experiences a totally different kinetic growth process compared to that of P123. If a low concentration of CTAB (below CMC) was applied, the hydrophobic hydrocarbon chain of CTAB was exposed as the monomer, which may preferably adhere on {111}s. The molecular arrangements of {111}s are almost along the hydrophobic aromatic planes, which might selectively adhere to the CTAB monomer (Figure S9b). It could slow down the growth rate of {111}s and result in the inhibition of the facet growth along the *x* axis at the early stage of self-assembly, thereby creating the elongated decahedral configuration. Subsequently, the

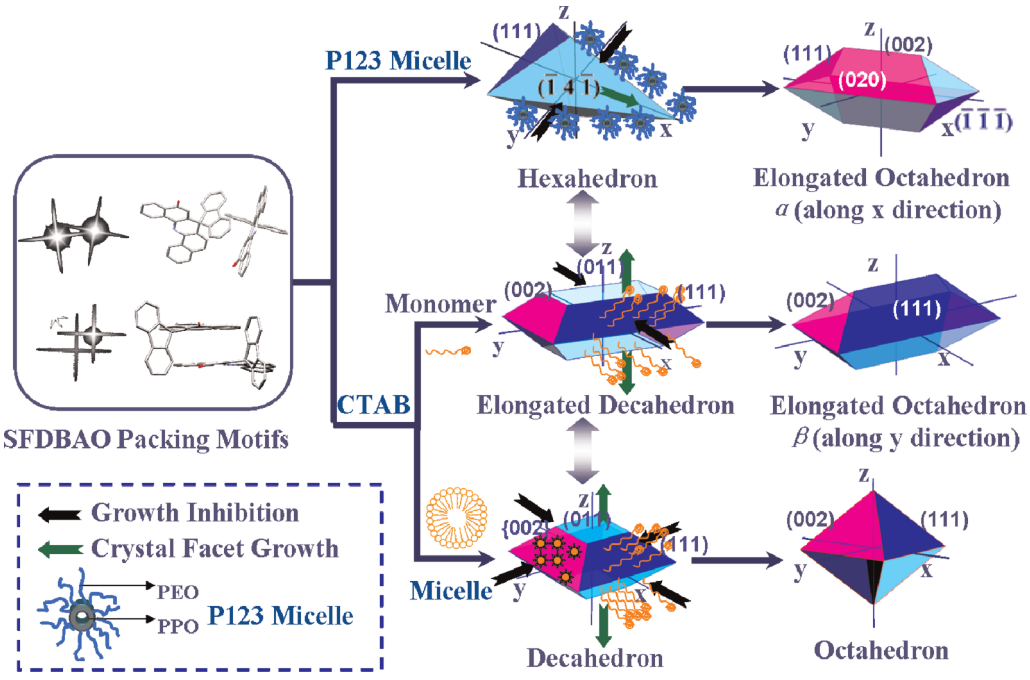

Scheme 2. Proposed self-assembled mechanism of the SFDBAO polyhedra.

elongated octahedron might consummate an elongated octahedron β, enduring the growth of {011}s in the *z* direction after aging for 48 h. However, in the case of higher CTAB concentrations, the CTAB chains could tend to self-associate to form a spherical micelle with ammonium hydrophilic polar groups on the shell. The arrangement of ketone groups of the SFDBAO molecule is parallel with both {002}s and {020}s in Figure S10, which exposed the hydrophilic facets during crystal growth. The selective adhesion of the isotropic CTAB micelles on the hydrophilic {002}s and {020}s could take charge of further inhibition growth along the *x* axis, except for that of the CTAB monomer. Growth of {111}s and {002}s is inhibited, and as a result, the decahedra are formed. The persistent growth along the *z* direction results in the octahedra. The big size of elongated octahedron β (elongated decahedron) was attributed to the selective adhesion of the CTAB monomer (below the CMC) in the hydrophilic facets and resulted in the quick growth along the *y* direction. Tuning C_{CTAB} from 1 to 8 mg/mL, exceeding the CMC and hardly increasing the effect of solubilization, the supersaturation degree of SFDBAO was very close to each other. However, growth inhibitions along both directions will cause more nucleus and finally growth into a much smaller octahedron.[27,32,34,36] A nucleus may grow into different immediate polyhedra by tuning the hydrophobic (or hydrophilic) adhesion forces and the surface energy of growing facets. These as-prepared hexahedra, elongated decahedra, and decahedra might transform into each other, presumably, by adjusting the balance of interactions between SFDBAO and surfactant molecules at the interface, under the assistance of surfactants.

CONCLUSIONS

In summary, employing supramolecular steric hindrance and kinetically controllable effect, we have successfully self-assembled the cruciform-shaped SFDBAO molecules into crystalline micro/nanocrystals with diverse morphologies such as hexahedra, elongated octahedra, octahedra, decahedra, and elongated decahedra with the assistance of P123 and CTAB surfactants. The kinetic evolution of polyhedra is further investigated with SEM, TEM, SAED, and XRD by tuning the growth parameters. The possible mechanism was also proposed as the different preference of selective adhesions of P123 and CTAB micelles (or monomer) on crystal facets to equilibrate the $\pi\cdots\pi$ stacking interactions between SFDBAO molecules and the interactions between surfactants and SFDBAO molecules, leading to the balance of growth rate in different directions. The unique cruciform-shaped SAHs might provide a facile strategy to design the highly symmetric polyhedra of organic materials from "bottom up", which could be exploited as the building block for micro/nano-optoelectronic devices.

EXPERIMENTAL SECTION

Chemical and Materials. Spiro[fluorene-9,7′-dibenzo[*c*,*h*]acridine]. SFDBA was synthesized according to the reported precedure.[53−56] Tetrahydrofuran (THF) was purchased from Alfa Aesar company (Germany) and VWR Singapore PTE Ltd. (France). Poly(ethylene glycol)-*block*-poly(propyleneglycol)-*block*-poly(ethylene glycol) (P123) and cetyltrimethylammonium bromide (CTAB) were purchased from Aldrich Company (Germany). All chemicals

were used directly without further purification. Ultrapure water was obtained from the Millipore S. A. 67120 apparatus (France) with a resistivity of 18.2 MΩ cm. All chemicals were used as received without further purification.

Synthesis of Spiro[fluorene-9,7′-dibenzo[*c*,*h*]acridine]-5′-one (SFDBAO). In a round-bottom flask, spiro[fluorene-9,7′-dibenzo[*c*,*h*]acridine] (SFDBA) (0.50 g, 1.16 mmol) was dissolved in acetone (300 mL), and the mixture was stirred in air atmosphere with sunlight irradiation under for 6 h to produce spiro[fluorene-9,7′-dibenzo[*c*,*h*]acridine]-5′-one (SFDBAO). The crude product was purified by flash column chromatography using CH_2Cl_2/petroleum ether = 1:3 as eluent to give SFDBAO (0.39 g) as a red solid: yield 76%; GC-MS (EI-*m*/*z*) calcd for $C_{33}H_{19}NO^+$ $[M]^+$ 445.15, found 445.00; ^{1}H NMR (400 MHz, $CDCl_3$, ppm) δ 9.27 (d, J = 8.7 Hz, 1H), 9.05 (d, J = 8.7 Hz, 1H), 8.13 (d, J = 8.6 Hz, 1H), 7.90−7.83 (m, 3H), 7.76 (t, J = 8.8 Hz, 2H), 7.67 (t, J = 8.1 Hz, 1H), 7.59 (t, J = 7.5 Hz, 1H), 7.54 (d, J = 8.5 Hz, 1H), 7.43 (t, J = 7.5 Hz, 2H), 7.20 (t, J = 7.5 Hz, 2H), 7.03 (d, J = 7.6 Hz, 2H), 6.56 (d, J = 8.5 Hz, 1H), 6.04 (s, 1H); ^{13}C NMR (100 MHz, $CDCl_3$, ppm) δ 184.55, 151.70, 150.04, 145.43, 140.84, 137.83, 135.65, 133.67, 132.79, 132.27, 131.42, 130.81, 130.31, 128.92, 128.88, 128.68, 127.77, 127.28, 126.77, 125.99, 125.35, 124.85, 124.65, 123.81, 120.74, 57.79. Anal. Calcd for $C_{33}H_{19}NO$: C, 89.04; H, 4.30; N, 3.15. Found: C, 89.07; H, 4.28; N, 3.18.

Assembly of Supramolecules. SFDBAO was dissolved in THF to form a concentration range from 0.5 to 2 mM. This solution (from 0.5 to 1.5 mL) was injected into 5 mL of high purity water or aqueous surfactant (in different concentrations) with stirring, and the water was maintained at the room temperature of 20 °C. After being stirred for 5 min, the sample was left undisturbed for about 4−48 h to stabilize the nanostructures (several samples need a longer aging time). The samples suffered subsequent separation *via* decanting of the supernatant liquid after centrifugation and were washed with pure water several times.

Characterization. ^{1}H NMR spectra in $CDCl_3$ were recorded at 400 MHz using a Varian Mercury 400 plus spectrometer. The FTIR spectra (KBr pellets) were obtained on a PerkinElmer spectrum GX. For scanning electron microscopic (SEM) studies, a drop of 20 μL of samples was placed onto silicon substrates, and the solvent was left to evaporate. The samples were then examined with a field emission SEM (JSM-6340F, JEOL) at an accelerating voltage of 5 kV. The TEM and SAED studies were performed in a JEM 2010F JEOL, operating at an accelerating voltage of 100 kV. A drop of 20 μL of as-prepared colloidal dispersion was deposited on a carbon-coated copper grid. The X-ray diffraction (XRD) patterns were performed on a Bruker D8 X-ray diffractometer with Cu Kα radiation (λ = 1.54050 Å). The operating 2θ angle ranges from 5 to 70°, with the step length of 0.025°.

Conflict of Interest: The authors declare no competing financial interest.

Acknowledgment. The project was supported by the National Key Basic Research Program of China (973) (2009CB930600), National Natural Science Foundation of China (20774043, 20704023, 20974046, 60876010, 21101095), Key Project of the Ministry of Education of China (707032, 208050), Natural Science Foundation of Jiangsu Province, China (BK2008053, SJ209003, 10KJB510013), Program for New Century Excellent Talents in University (NCET-11-0992), Funding of Jiangsu Innovation Program for Graduate Education (Grant No. CXZZ11_0413). Q.Z. thanks the funding support from the NTU start-up grant, AcRF Tier 1 (RG 18/09) from MOE, CREATE program (Nanomaterials for Energy and Water Management) from NRF, and New Initiative Fund from NTU, Singapore.

Supporting Information Available: NMR, FTIR characterizations, SEM, and details of SAED analysis for the SFDBAO-based micro/nanopolyhedra. This material is available free of charge *via* the Internet at http://pubs.acs.org.

REFERENCES AND NOTES

1. Tessler, N.; Denton, G. J.; Friend, R. H. Lasing from Conjugated-Polymer Microcavities. *Nature* **1996**, *382*, 695–697.
2. Kim, Y.; Cook, S.; Tuladhar, S. M.; Choulis, S. A.; Nelson, J.; Durrant, J. R.; Bradley, D. D. C.; Giles, M.; McCulloch, I.; Ha, C. S.; Ree, M. A Strong Regioregularity Effect in Self-Organizing Conjugated Polymer Films and High-Efficiency Polythiophene: Fullerene Solar Cells. *Nat. Mater.* **2006**, *5*, 197–203.
3. Krauss, T. F.; DeLaRue, R. M.; Brand, S. Two-Dimensional Photonic-Bandgap Structures Operating at Near Infrared Wavelengths. *Nature* **1996**, *383*, 699–702.
4. Atwater, H. A.; Polman, A. Plasmonics for Improved Photovoltaic Devices. *Nat. Mater.* **2010**, *9*, 205–213.
5. Koller, D. M.; Hohenau, A.; Ditlbacher, H.; Galler, N.; Reil, F.; Aussenegg, F. R.; Leitner, A.; List, E. J. W.; Krenn, J. R. Organic Plasmon-Emitting Diode. *Nat. Photonics* **2008**, *2*, 684–687.
6. O'Carroll, D.; Lieberwirth, I.; Redmond, G. Microcavity Effects and Optically Pumped Lasing in Single Conjugated Polymer Nanowires. *Nat. Nanotechnol.* **2007**, *2*, 180–184.
7. Huang, C.; Li, Y.; Song, Y.; Li, Y.; Liu, H.; Zhu, D. Ordered Nanosphere Alignment of Porphyrin for the Improvement of Nonlinear Optical Properties. *Adv. Mater.* **2010**, *22*, 3532–3536.
8. Cui, S.; Liu, H.; Gan, L.; Li, Y.; Zhu, D. Fabrication of Low-Dimension Nanostructures Based on Organic Conjugated Molecules. *Adv. Mater.* **2008**, *20*, 2918–2925.
9. Zheng, J. Y.; Yan, Y.; Wang, X.; Zhao, Y. S.; Huang, J.; Yao, J. Wire-on-Wire Growth of Fluorescent Organic Heterojunctions. *J. Am. Chem. Soc.* **2012**, *134*, 2880–2883.
10. Zhang, C.; Zou, C.-L.; Yan, Y.; Hao, R.; Sun, F.-W.; Han, Z.-F.; Zhao, Y. S.; Yao, J. Two-Photon Pumped Lasing in Single-Crystal Organic Nanowire Exciton Polariton Resonators. *J. Am. Chem. Soc.* **2011**, *133*, 7276–7279.
11. Zhao, Y. S.; Fu, H.; Hu, F.; Peng, A. D.; Yao, J. Multicolor Emission from Ordered Assemblies of Organic 1D Nanomaterials. *Adv. Mater.* **2007**, *19*, 3554–3558.
12. Zhang, X.; Jie, J.; Zhang, W.; Zhang, C.; Luo, L.; He, Z.; Zhang, X.; Zhang, W.; Lee, C.; Lee, S. Photoconductivity of a Single Small-Molecule Organic Nanowire. *Adv. Mater.* **2008**, *20*, 2427–2432.
13. Zhang, X.; Zhang, X.; Wang, B.; Zhang, C.; Chang, J. C.; Lee, C. S.; Lee, S.-T. One- or Semi-Two-Dimensional Organic Nanocrystals Induced by Directional Supramolecular Interactions. *J. Phys. Chem. C* **2008**, *112*, 16264–16268.
14. Zhang, X.; Zhang, X.; Zou, K.; Lee, C.-S.; Lee, S.-T. Single-Crystal Nanoribbons, Nanotubes, and Nanowires from Intramolecular Charge-Transfer Organic Molecules. *J. Am. Chem. Soc.* **2007**, *129*, 3527–3532.
15. Dong, H.; Jiang, S.; Jiang, L.; Liu, Y.; Li, H.; Hu, W.; Wang, E.; Yan, S.; Wei, Z.; Xu, W.; Gong, X. Nanowire Crystals of a Rigid Rod Conjugated Polymer. *J. Am. Chem. Soc.* **2009**, *131*, 17315–17320.
16. Tang, Q.; Li, H.; Liu, Y.; Hu, W. High-Performance Air-Stable n-Type Transistors with an Asymmetrical Device Configuration Based on Organic Single-Crystalline Submicrometer/Nanometer Ribbons. *J. Am. Chem. Soc.* **2006**, *128*, 14634–14639.
17. Ando, S.; Murakami, R.; Nishida, J.-I.; Tada, H.; Inoue, Y.; Tokito, S.; Yamashita, Y. n-Type Organic Field-Effect Transistors with Very High Electron Mobility Based on Thiazole Oligomers with Trifluoromethylphenyl Groups. *J. Am. Chem. Soc.* **2005**, *127*, 14996–14997.
18. Sundar, V. C.; Zaumseil, J.; Podzorov, V.; Menard, E.; Willett, R. L.; Someya, T.; Gershenson, M. E.; Rogers, J. A. Elastomeric Transistor Stamps: Reversible Probing of Charge Transport in Organic Crystals. *Science* **2004**, *303*, 1644–1646.
19. Xiao, J.; Yin, Z.; Li, H.; Zhang, Q.; Boey, F.; Zhang, H.; Zhang, Q. Postchemistry of Organic Particles: When TTF Microparticles Meet TCNQ Microstructures in Aqueous Solution. *J. Am. Chem. Soc.* **2010**, *132*, 6926–6928.
20. Xiao, J.; Kusuma, D. Y.; Wu, Y.; Boey, F.; Zhang, H.; Lee, P. S.; Zhang, Q. Postchemistry of Organic Microrods: Thermopolymerization in Aqueous Solution. *Chem. Asian J.* **2011**, *6*, 801–803.
21. Xiao, J.; Yang, H.; Yin, Z.; Guo, J.; Boey, F.; Zhang, H.; Zhang, Q. Preparation, Characterization, and Photoswitching/Light-Emitting Behaviors of Coronene Nanowires. *J. Mater. Chem.* **2011**, *21*, 1423–1427.

22. Xiao, J.; Yin, Z.; Yang, B.; Liu, Y.; Ji, L.; Guo, J.; Huang, L.; Liu, X.; Yan, Q.; Zhang, H.; Zhang, Q. Preparation, Characterization, Physical Properties, and Photoconducting Behavior of Anthracene Derivative Nanowires. *Nanoscale* **2011**, *3*, 4720–4723.
23. Xiao, J.; Yang, B.; Wong, J. I.; Liu, Y.; Wei, F.; Tan, K. J.; Teng, X.; Wu, Y.; Huang, L.; Kloc, C.; Boey, F.; Ma, J.; Zhang, H.; Yang, H.; Zhang, Q. Synthesis, Characterization, Self-Assembly and Physical Properties of 11-Methyl-benzo-[*d*]pyreno[4,5-*b*]furan. *Org. Lett.* **2011**, *13*, 3004–3007.
24. Tao, A.; Sinsermsuksakul, P.; Yang, P. Polyhedral Silver Nanocrystals with Distinct Scattering Signatures. *Angew. Chem., Int. Ed.* **2006**, *45*, 4597–4601.
25. Kim, F.; Connor, S.; Song, H.; Kuykendall, T.; Yang, P. Platonic Gold Nanocrystals. *Angew. Chem., Int. Ed.* **2004**, *43*, 3673–3677.
26. Cao, H.; Qian, X.; Wang, C.; Ma, X.; Yin, J.; Zhu, Z. High Symmetric 18-Facet Polyhedron Nanocrystals of Cu_7S_4 with a Hollow Nanocage. *J. Am. Chem. Soc.* **2005**, *127*, 16024–16025.
27. Tsung, C.-K.; Kuhn, J. N.; Huang, W.; Aliaga, C.; Hung, L.-I.; Somorjai, G. A.; Yang, P. Sub-10 nm Platinum Nanocrystals with Size and Shape Control: Catalytic Study for Ethylene and Pyrrole Hydrogenation. *J. Am. Chem. Soc.* **2009**, *131*, 5816–5822.
28. Jun, Y.-W.; Lee, J.-H.; Choi, J.-S.; Cheon, J. Symmetry-Controlled Colloidal Nanocrystals: Nonhydrolytic Chemical Synthesis and Shape Determining Parameters. *J. Phys. Chem. B* **2005**, *109*, 14795–14806.
29. Weissbuch, I.; Popovitzbiro, R.; Lahav, M.; Leiserowitz, L. Understanding and Control of Nucleation, Growth, Habit, Dissolution and Structure of 2-Dimensiongal and 3-Dimensional Crystals Using Tailor-Made Auxiliaries. *Acta Crystallogr., Sect. B* **1995**, *51*, 115–148.
30. Hollingsworth, M. D. Crystal Engineering: From Structure to Function. *Science* **2002**, *295*, 2410–2413.
31. Peresypkina, E. V.; Blatov, V. A. Topology of Molecular Packings in Organic Crystals. *Acta Crystallogr., Sect. B* **2000**, *56*, 1035–1045.
32. Yin, Y.; Alivisatos, A. P. Colloidal Nanocrystal Synthesis and the Organic–Inorganic Interface. *Nature* **2005**, *437*, 664–670.
33. Pileni, M. P. The Role of Soft Colloidal Templates in Controlling the Size and Shape of Inorganic Nanocrystals. *Nat. Mater.* **2003**, *2*, 145–150.
34. Zhang, X.; Dong, C.; Zapien, J. A.; Ismathullakhan, S.; Kang, Z.; Jie, J.; Zhang, X.; Chang, J. C.; Lee, C.-S.; Lee, S.-T. Polyhedral Organic Microcrystals: From Cubes to Rhombic Dodecahedra. *Angew. Chem., Int. Ed.* **2009**, *48*, 9121–9123.
35. Kang, L.; Fu, H.; Cao, X.; Shi, Q.; Yao, J. Controlled Morphogenesis of Organic Polyhedral Nanocrystals from Cubes, Cubooctahedrons, to Octahedrons by Manipulating the Growth Kinetics. *J. Am. Chem. Soc.* **2011**, *133*, 1895–1901.
36. Moulton, B.; Zaworotko, M. J. From Molecules to Crystal Engineering: Supramolecular Isomerism and Polymorphism in Network Solids. *Chem. Rev.* **2001**, *101*, 1629–1658.
37. Liu, Y.; Tang, Z. Nanoscale Biocoordination Polymers: Novel Materials from an Old Topic. *Chem.—Eur. J.* **2012**, *18*, 1030–1037.
38. Liu, Y.; Ma, W.; Liu, W.; Li, C.; Liu, Y.; Jiang, X.; Tang, Z. Silver(I)–Glutathione Biocoordination Polymer Hydrogel: Effective Antibacterial Activity and Improved Cytocompatibility. *J. Mater. Chem.* **2011**, *21*, 19214–19218.
39. Li, C.; Deng, K.; Tang, Z.; Jiang, L. Twisted Metal-Amino Acid Nanobelts: Chirality Transcription from Molecules to Frameworks. *J. Am. Chem. Soc.* **2010**, *132*, 8202–8209.
40. Madueno, R.; Raisanen, M. T.; Silien, C.; Buck, M. Functionalizing Hydrogen-Bonded Surface Networks with Self-Assembled Monolayers. *Nature* **2008**, *454*, 618–621.
41. Hirst, A. R.; Escuder, B.; Miravet, J. F.; Smith, D. K. High-Tech Applications of Self-Assembling Supramolecular Nanostructured Gel-Phase Materials: From Regenerative Medicine to Electronic Devices. *Angew. Chem., Int. Ed.* **2008**, *47*, 8002–8018.
42. Yamamoto, Y.; Fukushima, T.; Suna, Y.; Ishii, N.; Saeki, A.; Seki, S.; Tagawa, S.; Taniguchi, M.; Kawai, T.; Aida, T. Photoconductive Coaxial Nanotubes of Molecularly Connected Electron Donor and Acceptor Layers. *Science* **2006**, *314*, 1761–1764.
43. Hoeben, F. J. M.; Jonkheijm, P.; Meijer, E. W.; Schenning, A. P. H. J. About Supramolecular Assemblies of π-Conjugated Systems. *Chem. Rev.* **2005**, *105*, 1491–1546.
44. Tevis, I. D.; Palmer, L. C.; Herman, D. J.; Murray, I. P.; Stone, D. A.; Stupp, S. I. Self-Assembly and Orientation of Hydrogen-Bonded Oligothiophene Polymorphs at Liquid–Membrane–Liquid Interfaces. *J. Am. Chem. Soc.* **2011**, *133*, 16486–16494.
45. Kwon, S.; Jeon, A.; Yoo, S. H.; Chung, I. S.; Lee, H.-S. Unprecedented Molecular Architectures by the Controlled Self-Assembly of a β-Peptide Foldamer. *Angew. Chem., Int. Ed.* **2010**, *122*, 8408–8412.
46. Kwon, S.; Shin, H. S.; Gong, J.; Eom, J.-H.; Jeon, A.; Yoo, S. H.; Chung, I. S.; Cho, S. J.; Lee, H.-S. Self-Assembled Peptide Architecture with a Tooth Shape: Folding into Shape. *J. Am. Chem. Soc.* **2011**, *133*, 17618–17621.
47. Hasell, T.; Chong, S. Y.; Jelfs, K. E.; Adams, D. J.; Cooper, A. I. Porous Organic Cage Nanocrystals by Solution Mixing. *J. Am. Chem. Soc.* **2011**, *134*, 588–598.
48. Liu, H.; Xu, J.; Li, Y.; Li, Y. Aggregate Nanostructures of Organic Molecular Materials. *Acc. Chem. Res.* **2010**, *43*, 1496–1508.
49. Li, R.; Hu, W.; Liu, Y.; Zhu, D. Micro- and Nanocrystals of Organic Semiconductors. *Acc. Chem. Res.* **2010**, *43*, 529–540.
50. Zhao, Y. S.; Fu, H.; Peng, A.; Ma, Y.; Xiao, D.; Yao, J. Low-Dimensional Nanomaterials Based on Small Organic Molecules: Preparation and Optoelectronic Properties. *Adv. Mater.* **2008**, *20*, 2859–2876.
51. Yang, B.; Xiao, J.; Wong, J. I.; Guo, J.; Wu, Y.; Ong, L.; Lao, L. L.; Boey, F.; Zhang, H.; Yang, H. Y.; Zhang, Q. Shape-Controlled Micro/Nanostructures of 9,10-Diphenylanthracene (DPA) and Their Application in Light-Emitting Devices. *J. Phys. Chem. C* **2011**, *115*, 7924–7927.
52. Zhang, X.; Yuan, G.; Li, Q.; Wang, B.; Zhang, X.; Zhang, R.; Chang, J. C.; Lee, C.-S.; Lee, S.-T. Single-Crystal 9,10-Diphenylanthracene Nanoribbons and Nanorods. *Chem. Mater.* **2008**, *20*, 6945–6950.
53. Xie, L.-H.; Ling, Q.-D.; Hou, X.-Y.; Huang, W. An Effective Friedel–Crafts Postfunctionalization of Poly(*N*-vinylcarbazole) To Tune Carrier Transportation of Supramolecular Organic Semiconductors Based on π-Stacked Polymers for Nonvolatile Flash Memory Cell. *J. Am. Chem. Soc.* **2008**, *130*, 2120–2121.
54. Gholami, M.; Tykwinski, R. R. Oligomeric and Polymeric Systems with a Cross-Conjugated π-Framework. *Chem. Rev.* **2006**, *106*, 4997–5027.
55. Xie, L.-H.; Hou, X.-Y.; Hua, Y.-R.; Huang, Y.-Q.; Zhao, B.-M.; Liu, F.; Peng, B.; Wei, W.; Huang, W. An Effective Strategy To Tune Supramolecular Interaction *via* a Spiro-Bridged Spacer in Oligothiophene-S,S-Dioxides and Their Anomalous Photoluminescent Behavior. *Org. Lett.* **2007**, *9*, 1619–1622.
56. Xie, L.-H.; Liu, F.; Tang, C.; Hou, X.-Y.; Hua, Y.-R.; Fan, Q.-L.; Huang, W. Unexpected One-Pot Method to Synthesize Spiro[fluorene-9,9-xanthene] Building Blocks for Blue-Light-Emitting Materials. *Org. Lett.* **2006**, *8*, 2787–2790.
57. The SFDBAO polyhedra were modeled with WinXMorph V1.51.
58. Kaminsky, W. WinXMorph: A Computer Program To Draw Crystal Morphology, Growth Sectors and Cross Sections with Export Files in VRML V2.0 Utf8-Virtual Reality Format. *J. Appl. Crystallogr.* **2005**, *38*, 566–567.
59. Kaminsky, W. From CIF to Virtual Morphology Using the WinXMorph Program. *J. Appl. Crystallogr.* **2007**, *40*, 382–385.
60. Alexandridis, P.; Holzwarth, J. F.; Hatton, T. A. Micellization of Poly(ethylene oxide)–Poly(propylene oxide)–Poly(ethylene oxide) Triblock Copolymers in Aqueous Solutions: Thermodynamics of Copolymer Association. *Macromolecules* **1994**, *27*, 2414–2425.
61. Mitchard, N. M.; Beezer, A. E.; Mitchell, J. C.; Armstrong, J. K.; Chowdhry, B. Z.; Leharne, S.; Buckton, G. Thermodynamic

Analysis of Scanning Calorimetric Transitions Observed for Dilute Aqueous Solutions of ABA Block Copolymers. *J. Phys. Chem.* **1992**, *96*, 9507–9512.
62. Linse, P. Phase Behavior of Poly(ethylene oxide)–Poly(propylene oxide) Block Copolymers in Aqueous Solution. *J. Phys. Chem.* **1993**, *97*, 13896–13902.
63. Aguiar, J.; Carpena, P.; Molina-Bolivar, J. A.; Ruiz, C. C. On the Determination of the Critical Micelle Concentration by the Pyrene 1:3 Ratio Method. *J. Colloid Interface Sci.* **2003**, *258*, 116–122.
64. Modaressi, A.; Sifaoui, H.; Grzesiak, B.; Solimando, R.; Domanska, U.; Rogalski, M. CTAB Aggregation in Aqueous Solutions of Ammonium Based Ionic Liquids; Conductimetric Studies. *Colloids Surf. A* **2007**, *296*, 104–108.
65. Hollingsworth, M. D. Crystal Engineering: From Structure to Function. *Science* **2002**, *295*, 2410–2413.
66. Liu, X. Y.; Boek, E. S.; Briels, W. J.; Bennema, P. Prediction of Crystal Growth Morphology Based on Structural Analysis of the Solid–Fluid Interface. *Nature* **1995**, *374*, 342–345.
67. Huang, L.; Liao, Q.; Shi, Q.; Fu, H.; Ma, J.; Yao, J. Rubrene Micro-Crystals from Solution Routes: Their Crystallography, Morphology and Optical Properties. *J. Mater. Chem.* **2010**, *20*, 159–166.
68. Lei, Y.; Liao, Q.; Fu, H.; Yao, J. Phase- and Shape-Controlled Synthesis of Single Crystalline Perylene Nanosheets and Its Optical Properties. *J. Phys. Chem. C* **2009**, *113*, 10038–10043.
69. Linse, P.; Malmsten, M. Temperature-Dependent Micellization in Aqueous Block Copolymer Solutions. *Macromolecules* **1992**, *25*, 5434–5439.
70. Mortensen, K.; Pedersen, J. S. Structural Study on the Micelle Formation of Poly(ethylene oxide)–Poly(propylene oxide)–Poly(ethylene oxide) Triblock Copolymer in Aqueous Solution. *Macromolecules* **1993**, *26*, 805–812.